PAPER

Check for updates

Mechanistic studies of atomic layer deposition on oxidation catalysts – AlO$_x$ and PO$_x$ deposition†

Kristian Knemeyer, [a] Mar Piernavieja Hermida,[a] Piyush Ingale, [a] Johannes Schmidt,[b] Jutta Kröhnert,[c] Raoul Naumann d'Alnoncourt, ★[a] Matthias Driess [ab] and Frank Rosowski[ad]

Atomic layer deposition is a rising technique for catalyst synthesis and modification. Typically, the focus of ALD in catalysis is on supported metal nanoparticles. Here, the authors give mechanistic insights into the ALD of oxides on redox active catalysts by a combination of *in situ* analytics, such as XPS, DRIFTS and gravimetric measurements. Phosphorus oxide and aluminum oxide were deposited on divanadium pentoxide powder in a fixed bed reactor. In contrast to the generally accepted concepts, the first half cycle does not proceed over surface hydroxyl groups but involves redox chemistry between the precursor and the vanadium atoms, as shown by ^{31}P-SSNMR and XPS. For PO$_x$ deposition, a temperature step from 150 °C in the first half cycle to 450 °C in the second half cycle is needed to obtain linear mass gain per cycle as the remaining ligands are combusted and reduced vanadium atoms are reoxidized. Homogeneous deposition was confirmed by STEM-EDX and XRD showing no additional phases, despite performing up to 10 ALD cycles. Even the well-known process of alumina ALD confirms the involvement of reduction–oxidation reactions between the ALD precursor and the substrate V$_2$O$_5$. However, redox chemistry can be suppressed for alumina ALD at low temperatures of 50 °C. Therefore, this study shows that ALD on oxidation catalysts is complex and thus the developed ALD processes are unusual compared to ALD on typical supports, such as SiO$_2$ or Al$_2$O$_3$.

Introduction

Atomic layer deposition (ALD) is a sequential thin film deposition technique with high dispersion, uniform coating, precise thickness control and high degree of reproducibility. ALD is capable of depositing nearly any element of the periodic table on flat substrates and numerous processes are already industrially applied, *e.g.* in the field of microelectronics. In recent years, ALD received huge attention in different fields such as battery or catalyst synthesis due to the aforementioned beneficial characteristics. Besides flat substrates it is possible to deposit functional materials on powders, such as VPO$_4$[1] or Li$_3$PO$_4$[2] for battery applications or enhance the lifetime of batteries by Al$_2$O$_3$ coatings.[3]

^{a} *BasCat—UniCat BASF JointLab, Technische Universität Berlin, Hardenbergstraße 36, 10623 Berlin, Germany. E-mail: r.naumann@bascat.tu-berlin.de*

^{b} *Institut für Chemie, Technische Universität Berlin, Straße des 17, Juni 135, 10623 Berlin, Germany*

^{c} *Department of Inorganic Chemistry, Fritz-Haber-Institut der Max-Planck-Gesellschaft, Faradayweg 4-6, 14195 Berlin, Germany*

^{d} *BASF SE, Process Research and Chemical Engineering, Carl-Bosch-Straße 38, 67056 Ludwigshafen, Germany*

† Electronic supplementary information (ESI) available: Growth curves, XRD, XPS, STEM-EDX, and ICP-OES. See DOI: 10.1039/d0cp02572k

Furthermore, catalytically active elements can be deposited on almost every typical catalyst support, such as SiO$_2$, Al$_2$O$_3$, TiO$_2$ or ZrO$_2$.[4,5] Typically, bottom up catalyst synthesis *via* ALD aims at supported noble metals[6–8] or metal oxides.[9–11] Modifications of conventionally prepared catalysts are conducted *e.g.* by alumina overcoating to prevent sintering[12] or leaching.[13] However, additional challenges for ALD on powders have to be overcome. Reactor geometries are changed from overflow type reactors to fluidized or fixed bed reactors to overcome diffusion limitations. *In situ* process monitoring and growth determination on flat substrates is easy *via* spectroscopic ellipsometry[14] or with a quartz crystal microbalance[15] but neither of these methods can be directly used for powders and therefore need to be substituted with mass spectrometry or a magnetic suspension balance.[16] Additionally, one big difference between catalyst synthesis and microelectronics by ALD is the desired film thickness which is adjusted by the number of ALD cycles. ALD for microelectronics often aims for relative thick films in the range of nanometers up to micrometres which is realised by thousands of ALD cycles.[8,17] Whereas, in catalysis sub-monolayers,[18,19] single sites[20] or nanoparticles[21] are required and achieved by several ALD cycles. Despite non-ideal growth behaviour in the first cycles, such as nucleation delay,[22,23] mechanistic investigations on these phenomena are rarely

This journal is © the Owner Societies 2020

Phys. Chem. Chem. Phys., 2020, **22**, 17999–18006 | 17999

made. In fact, the first several ALD cycles are highly important to understand and control the deposition process and therefore the synthesized material. So far, the mechanistic consensus is that ALD proceeds over the reaction of, most often, a metal-organic precursor with the surface OH groups of the substrate forming a metal–oxygen bond by releasing a gaseous by-product in the first half cycle. The second half cycle proceeds by adding an oxidizing reactant to generate new hydroxyl groups.[5,24–26] However, these mechanistic insights are almost always given with respect to non-reducible supports on which the catalytic active species are being deposited. Depositing catalytic active layers on typical catalyst supports is not always straightforward as there is either no known process to obtain the desired catalytic active layer or the process is not applicable to porous powders. For example, T. Dobbelaere et al. developed an ALD process for vanadium phosphate on flat substrates involving O_2 plasma.[1] In fact, plasma has the drawback of surface recombination and might not be suitable for ALD on powders, especially in fixed bed geometry or with porous powders.[27,28] Therefore, surface modification of existing bulk catalysts is in some cases the only option to obtain the desired surface layer. However, bulk catalysts may contain additional reactive surface sites besides hydroxyl groups, leading to untypical ALD behaviour, especially for redox active oxidation catalysts as shown in this paper.

Here, we investigate an unusual ALD process of phosphorus oxide on divanadium pentoxide by investigating the reaction mechanism with multiple *in situ* analytics. In addition, the same methods were applied for alumina ALD on V_2O_5 and led to the conclusion that both processes undergo unexpected growth behaviour which needs to and can be controlled.

Experimental

Chemicals

Divanadium pentoxide (V_2O_5, 99.9%, Sigma Aldrich) was sieved to the fraction of 100–200 μm prior to use as substrate. Trimethyl aluminum (Al(CH$_3$)$_3$, TMA, electronic grade, >99.99%, Sigma-Aldrich) and water (H_2O, CHROMASOLV®, for HPLC, Riedel-de Haën) served as precursor for aluminum oxide ALD and were used without further purification. Trimethoxy phosphine (P(O(CH$_3$)$_3$), TMPT, 99.99%, Sigma-Aldrich) and high purity oxygen (O_2, 99.999%) served as precursor for phosphorous oxide ALD and were used without further purification. High purity nitrogen, argon and helium (99.999%) acted as carrier and purging gas.

Atomic layer deposition

ALD was performed in a fixed bed geometry at atmospheric pressure in either a magnetic suspension balance or in a quartz tube on divanadium pentoxide. The setup is described in more detail elsewhere.[16] Phosphorus oxide ALD was performed by saturating a constant N_2 stream of 25 mL min^{-1} with trimethoxy phosphine at 60 °C, diluting it in additional 25 mL min^{-1} of N_2 and then depositing it at 150 °C in the first half cycle until saturation. Oxygen served as the reactant in the second half cycle

with a flow of 10 mL min^{-1} diluted in 40 mL min^{-1} of He at 150 °C or at 450 °C until saturation. Up to ten ALD cycles of PO$_x$ were performed. Up to six cycles of aluminum oxide ALD were performed by saturating a constant N_2 stream of 25 mL min^{-1} with trimethyl aluminum heated to 50 °C, diluting it in additional 25 mL min^{-1} of N_2 followed by deposition at 150 °C or 50 °C. Water was introduced in the second half cycle by constant saturation of 50 mL min^{-1} He at room temperature. The second half cycle followed thermal treatment in 10 mL min^{-1} oxygen diluted in 40 mL min^{-1} He at 450 °C. Between all half cycles, the reactor was purged with 50 mL min^{-1} of Ar.

Characterization

N_2 physisorption. N_2 physisorption measurements were performed at liquid N_2 temperature on a Quantachrome autosorb-6B analyzer. Prior to the measurement, the samples were degassed in dynamic vacuum at 150 °C for 2 h. Full adsorption and desorption isotherms were measured. The specific surface area S_{BET} was calculated according to the multipoint Brunauer–Emmett–Teller (BET) method.

X-ray photoelectron spectroscopy (XPS). XPS measurements were performed using a ThermoScientific K-Alpha+ X-ray Photoelectron Spectrometer. All samples were analyzed using a micro-focussed, monochromated Al$_{K\alpha}$ X-ray source (1486.68 eV; 400 μm spot size). The analyzer had a pass energy of 200 eV (survey) and 50 eV (high resolution spectra), respectively. To prevent any localized charge buildup during analysis the K-Alpha+ charge compensation system was employed at all measurements. The samples were mounted on conductive carbon tape and the resulting spectra were analyzed using Avantage software from ThermoScientific.

Nuclear magnetic resonance (NMR). NMR spectra were recorded on a Bruker Avance 400 Solid State (400 MHz).

X-ray fluorescence spectroscopy (XRF). XRF was performed on a Bruker S4 Pioneer X-ray spectrometer. Samples were prepared by melting pellets with a ratio of 100 mg sample to 8.9 g of Li$_2$B$_4$O$_7$.

Inductively coupled plasma-optical emission spectroscopy (ICP-OES). ICP-OES was used to determine the P content on a Varian 720-ES. Solutions from the powders were prepared *via* acid digestion using saturated oxalic acid. The samples were treated at 60 °C for 12 h in an ultrasonic bath. The spectroscope was five-point calibrated with a commercially available, diluted standard for P.

Electron microscopy. Electron microscopy was performed using a FEI Talos F200X with an XFEG field emission gun and an acceleration voltage of 200 kV. STEM-EDX mappings were acquired with the SuperX system of 4 SDD EDX detectors.

Diffuse reflectance infrared Fourier transform spectroscopy (DRIFTS). DRIFTS was performed with a FTIR spectrometer (Cary 680) and DRIFTS cell (Harrick) with 512 scans and resolution of 2 cm^{-1}. The sample was assembled under inert conditions and the desired reactants were added to the substrate at varying temperatures (room temperature, 150 °C, and 450 °C.)

Powder X-ray diffraction (XRD). XRD measurements were performed in the Bragg–Brentano geometry on a D8 Advance II

18000 | *Phys. Chem. Chem. Phys.*, 2020, **22**, 17999–18006

This journal is © the Owner Societies 2020

theta/theta diffractometer (Bruker AXS), using Ni-filtered Cu K$_{\alpha1,2}$ radiation and a position sensitive energy dispersive LynxEye silicon strip detector. The sample powder was filled into the recess of a cup-shaped sample holder, the surface of the powder bed being flush with the sample holder edge (front loading).

Results and discussion

ALD of PO$_x$ on V$_2$O$_5$

Phosphorous oxide ALD was performed with trimethoxy phosphine and oxygen as reactants at 150 °C. In a magnetic suspension balance the mass gain was tracked *in situ* to obtain the growth per cycle (gpc) and determine the ALD window (shown as an example for the first cycle in Fig. 1a). In the first six ALD cycles self-limiting mass gain was observed in each half cycle but the gpc decreased with the cycle number from 0.34 wt% in the first cycle to 0.02 wt% in the sixth cycle (Fig. 1b). In the first cycle 0.12 wt% of P is deposited, which makes up 35% of the deposited
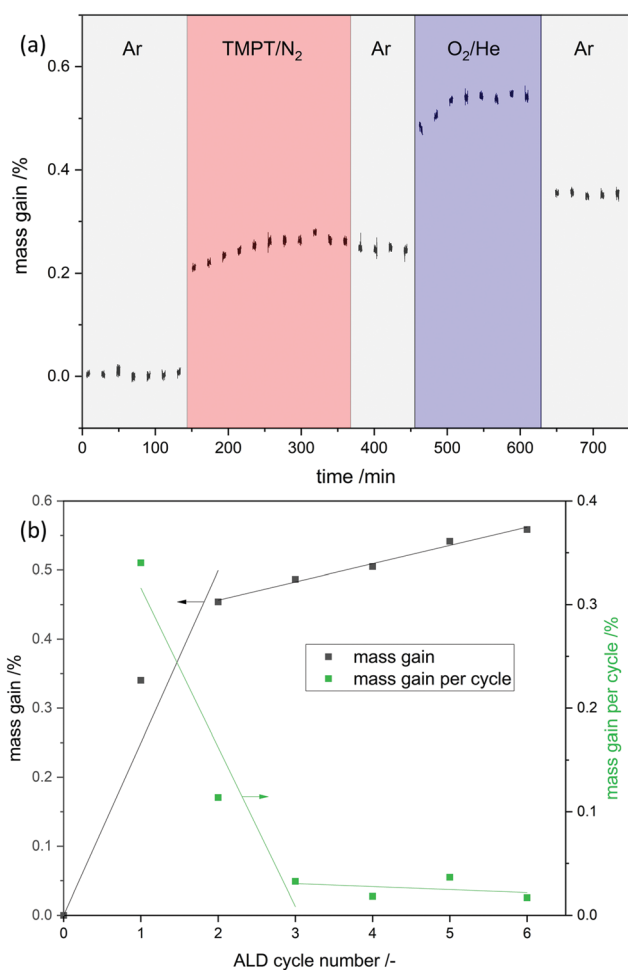
Fig. 1 (a) Mass gain as a function of time for PO$_x$-ALD in a magnetic suspension balance at 150 °C for cycle number one. N$_2$ was used as carrier gas for TMPT, Ar was used for purging, and O$_2$ was diluted in He. The dosing procedure is indicated at the top. Note: the apparent mass loss after the switch from O$_2$/He to Ar occurred due to the buoyancy effect. (b) Total mass gain and mass gain per cycle is shown.

Table 1 P loading determined by ICP-OES of synthesized PO$_x$/V$_2$O$_5$ with varying P-ALD cycles in the magnetic suspension balance (MSB) and fixed bed reactor (FB) and the surface area of the resulting sample

#cycle	P(MSB) wt%	P(FB) wt%	BET (m^2 g^{-1})
1	0.12	0.12	4.0
2	0.16	0.17	4.2
3	0.18	0.19	3.9
4	0.20	0.21	4.0
6	0.24	0.23	4.3

overall mass. This is comparable to the mass fraction of phosphorus in phosphoric acid (M(P)/M(H$_3$PO$_4$) = 32%). ICP-OES confirmed the increase of P with increasing cycle numbers.

After evaluating the process parameters in the magnetic suspension balance, the experimental conditions were transferred from the balance (1 mL) to a quartz tube reactor (30 mL). Scaling up the sample amount results in longer precursor dosing times based on higher total surface area. The scale up was successful as ICP-OES shows identical P loadings for each respective cycle in balance and quartz reactor (Table 1).

In addition, N$_2$ sorption measurements show no change the in surface area during ALD. In contrast to ALD on porous material on which the surface area drastically decreases due to the blocking of micropores[29] or even mesopores,[30] no change is expected for V$_2$O$_5$ as it contains no micro- or meso-pores and already has a relatively low surface area. Possible reason for the decrease in gpc is incomplete removal of ligands on phosphorus, which prevent further reaction or the previously reactive surface sites were not regenerated in the second half cycle. As the process does not lead to further significant deposition after the 3rd cycle it might not be called atomic layer deposition anymore. To remove residue ligands on the surface and recreate reactive surface sites, the procedure was performed at higher temperatures in the second half cycle (450 °C). Ten ALD cycles were performed and a linear gpc was achieved as shown by XRF measurements (Fig. 2). In addition,
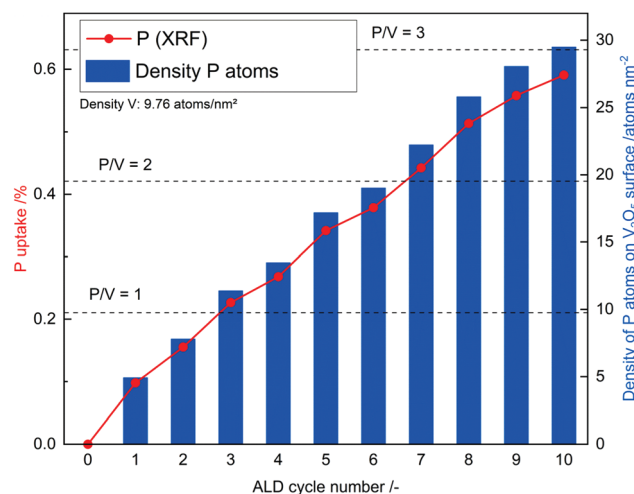
Fig. 2 Phosphorus uptake during ALD determined by XRF and the calculated density of P atoms on the surface of PO$_x$/V$_2$O$_5$.

This journal is © the Owner Societies 2020

Phys. Chem. Chem. Phys., 2020, **22**, 17999–18006 | **18001**

coverage by phosphorus was calculated by assuming primarily Frank–van-der-Merwe growth[31] and correlating the deposited amount of P to either surface hydroxyl group density or surface vanadium atom density (Fig. 2). Correlating P uptake in the very first cycle to the surface hydroxyl group density of 1.4 OH nm^{-2} [18] shows a P/OH ratio of 3.5. In contrast to the often in literature proposed ALD mechanism over surface OH-groups, PO_x-ALD has to undergo a different and/or additional mechanism as the amount of P exceeds the number of OH groups resulting in more than one monolayer coverage in one cycle. Physisorption of the precursor is excluded by the balance experiment as tailing would occur during purging with Ar. In addition, P is stable during post treatment at 450 °C in dry and wet synthetic air indicating covalent bonds on the surface and not just physisorption. Therefore, additional reactive surface sites must be considered, such as surface vanadium atoms. Instead of determining the P/OH ratio, P/V was determined. The number of vanadium atoms per nm^2 on the surface was calculated based on the ideal crystal structure of the (010) plane in V_2O_5 and found to be 9.76 V nm^{-2}.[32] Based on these assumptions, the first monolayer forms after the 3rd cycle, the second layer after the 7th and the third layer after the 10th cycle. The formation of additional phases was investigated on the prepared 1 cycle and 10 cycle samples by XRD (ESI,† Fig. S1) and STEM-EDX (Fig. 3 and ESI,† Fig. S2). However, XRD reflexes only show phase pure divanadium pentoxide which means that either no additional crystalline phases are formed or the formed crystallites are smaller than the detection limit of typically <3 nm.[33] STEM-EDX shows highly dispersed phosphorus on divanadium pentoxide for the 1 cycle and 10 cycle samples. This indicates layer-by-layer growth, as big islands of PO_x would most likely be visible in STEM-EDX mapping, also

revealing uncovered V_2O_5. Furthermore, island growth is likely to be excluded based on the observed linear growth per cycle. For island growth, the growth per cycle would exponentially increase in the first ALD cycles until a closed layer forms because of which the gpc remains constant.[34–38]

ALD – investigations of the mechanism

ALD mechanisms are not fully understood, as detailed physical and chemical analysis in the first few cycles are challenging due to sensitivity and resolution restrictions. In the very first ALD cycle, less than a monolayer is deposited which shows the need for highly sensitive analytics.

In situ DRIFTS experiments were conducted to understand the difference between applying reactor temperatures of 150 °C and 450 °C in the second half cycle (Fig. 4). Therefore, one sample was prepared by performing one half cycle of TMPT on V_2O_5 and then transferred under inert conditions to the DRIFTS cell. After the first half cycle the phosphorus precursor was chemisorbed on the vanadium surface as indicated by C–H vibrations (2964 cm^{-1}). Heating up to 150 °C in 20% oxygen does not lead to a loss of these C–H fragments, meaning the surface is still partially covered with ligands of the precursor. Additionally, the condensation of OH groups (3365 cm^{-1}) on the surface occurs, showing that hydroxyl groups do not contribute to further ALD cycles. However, heating up to 450 °C leads to formation of CO_2 (2345 cm^{-1}) and the C–H vibrations (2960 cm^{-1} and 2858 cm^{-1}) diminish. This leads to the conclusion that at 450 °C the organic ligands on the surface are combusted and new anchoring sites for the following ALD cycle are created. Therefore, linear gpc can only be achieved by combusting remaining ligands in the second half cycle.

To further investigate the surface species during PO_x-ALD solid-state magic angle spinning ^{31}P-NMR experiments were conducted at each step during ALD synthesis. After the first and second half cycle at 150 °C no ^{31}P-NMR signals are obtained (ESI,† Fig. S3 and S4), but once the sample was exposed to oxygen at 450 °C clear P signals are visible (Fig. 5). This suggests that the P-precursor is anchored *via* a redox reaction with V_2O_5 with the formation of V^{4+} in the first half cycle, as vanadium atoms in lower oxidation states than V^{5+} are paramagnetic. Once a ^{31}P-nucleus is in close proximity to paramagnetic vanadium species the line width increases drastically and signals cannot be observed anymore.[39] After the oxygen treatment at 450 °C a ^{31}P-NMR signal is observed due to reoxidation of the former paramagnetic vanadia species into diamagnetic V^{5+}. In addition, a hint for redox chemistry is already given by the color change of the catalyst. Before ALD, divanadium
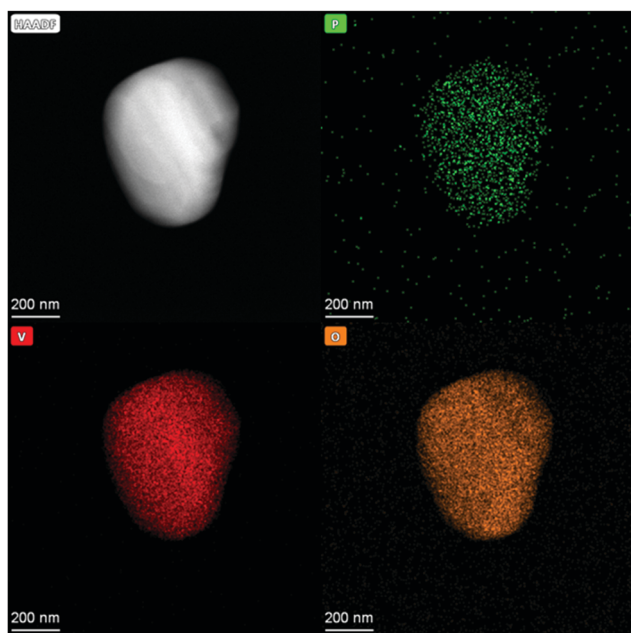

Fig. 3 HAADF image of PO_x/V_2O_5 prepared by 10 cycles of PO_x-ALD and STEM-EDX mappings of P, V and O.

Table 2 XPS summary of PO_x-ALD on V_2O_5 during each step in the first cycle by the determined ratio R

	R
V_2O_5 fresh	0.16
V_2O_5 calcined (450 °C)	0.11
PO_x/V_2O_5 1 half cycle	0.41
PO_x/V_2O_5 1 cycle (150 °C)	0.22
PO_x/V_2O_5 1 cycle (450 °C)	0.10

18002 | *Phys. Chem. Chem. Phys.*, 2020, **22**, 17999–18006
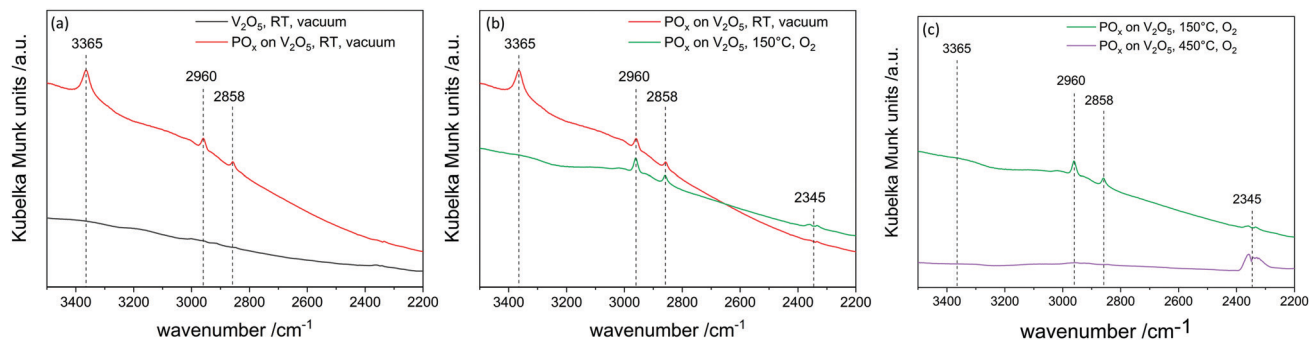
This journal is © the Owner Societies 2020

Fig. 4 *In situ* DRIFTS after the first half cycle of trimethoxy phosphine on V_2O_5. Shown are the comparisons between (left) fresh V_2O_5 and 1 half cycle TMPT; (middle) 1 half cycle TMPT and O_2 at 150 °C and (right) 1 full cycle at 150 °C and O_2 at 450 °C.
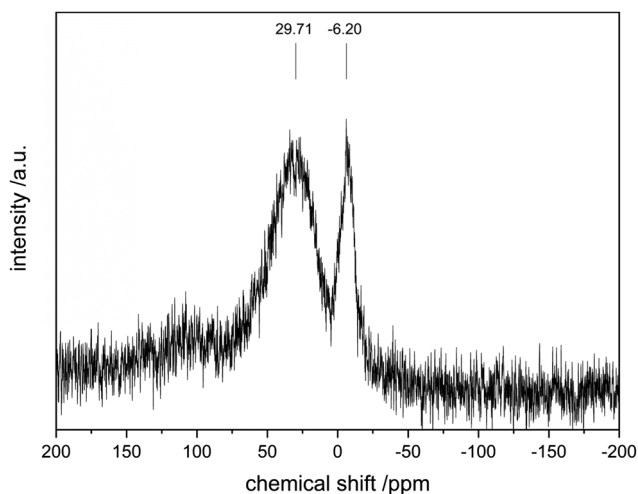

Fig. 5 ^{31}P-SSNMR of PO_x/V_2O_5 after 1 cycle PO_x-ALD. Note: the low signal to noise ratio is due to the low P loading (0.1%).

Fig. 6 XPS of PO_x/V_2O_5 after the first half cycle of PO_x-ALD. (a) O_{1s}, V_{2p} and (b) P_{2p} spectra.

pentoxide appears to be bright orange which then turns dark green after exposure to trimethoxy phosphine, which is comparable to the color of VO_2 (ESI,† Fig. S5). Dosing oxygen at 150 °C does not reverse the color but heating in O_2 at 450 °C does. Further studies of the oxidation states were performed by XPS experiments under inert conditions to investigate each step of the first cycle (Fig. 6). Overall, only vanadium atoms in the oxidation states of V^{5+} and V^{4+} were detected and a ratio R was calculated to describe the relative amount of reduced vanadium species in each synthesis step (Table 2).

$$R = \frac{V^{4+}}{V^{4+} + V^{5+}}$$

The bigger the R the more reduced vanadium is present within the scanned area of the sample. V_2O_5 is known to have oxygen vacancies[40,41] in the lattice structure and is therefore calcined at 450 °C in synthetic air to heal the defect sites before the usage in ALD. XPS shows that the calcined V_2O_5 has a lower amount of V^{4+} than fresh vanadia. Addition of the phosphorus precursor leads to reduction of the divanadium pentoxide as indicated by the increase of V^{4+} species. V^{3+} species are not found during XPS experiments. After the oxygen
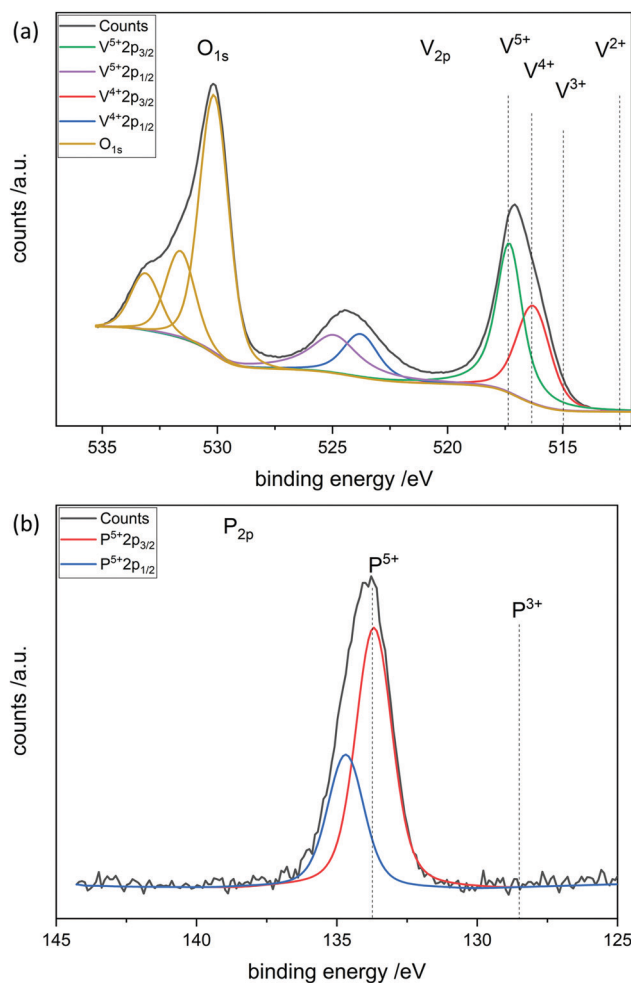
dosing at 150 °C part of the reduced vanadium is oxidized again to V^{5+}. Full reoxidation occurs in oxygen at 450 °C as R is similar to that of freshly calcined V_2O_5. The oxidation state of phosphorus reveals the immediate oxidation from P^{3+} to P^{5+} during the first half cycle. Thus, one molecule of trimethoxy phosphine can reduce two vanadium centers from V^{5+} to V^{4+} to give P^{5+}.

$$P^{3+} + 2V^{5+} \rightarrow P^{5+} + 2V^{4+}$$
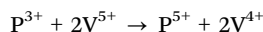
This is in good agreement with previously shown XRF results.

After the first half cycle a surface ratio of P/V = 0.50 is obtained, confirming that one P atom is located near two vanadium atoms, assuming deposition exclusively on the surface.

ALD of AlO_x on V_2O_5

Aluminum oxide ALD is the most prominent process in ALD history and therefore well investigated. The reaction mechanism is understood as a reaction between surface hydroxyl groups and trimethyl aluminum forming an oxygen aluminum bond while releasing methane in the first half cycle.[5,16] In the second half cycle, water regenerates hydroxyl groups by formation of more aluminum oxygen bonds and formation of methane. These ligand exchange reactions with surface hydroxyl groups typically do not cause changes in oxidation states, as aluminum remains in its maximum oxidation state.

First, deposition experiments of aluminum oxide on divanadium pentoxide were conducted in the magnetic suspension balance to investigate the growth behavior *in situ* for up to six cycles. The ALD sequence consists of addition of TMA followed by water with purging inbetween. In addition, a thermal treatment at 450 °C in O_2 is added after each cycle:

$$TMA-Ar-H_2O-Ar-O_2(450 \ °C)$$
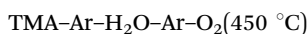
Each step shows a self-limiting mass gain (ESI,† Fig. S6) but the growth per cycle (gpc) decreases (Fig. 7). The contribution to the mass uptake of each step was calculated and results show that TMA has the highest impact on the gpc. Surprisingly, oxygen dosing at 450 °C contributes heavily to the mass gain, especially in the very first cycle with 25%. After the fourth cycle the impact of oxygen treatment decreases to almost zero. This indicates different growth modes during the deposition. First, aluminum oxide is deposited on divanadium pentoxide and with increasing cycle number aluminum oxide is deposited on itself as Al–OH groups are created. Three to four cycles of AlO_x-ALD lead to a
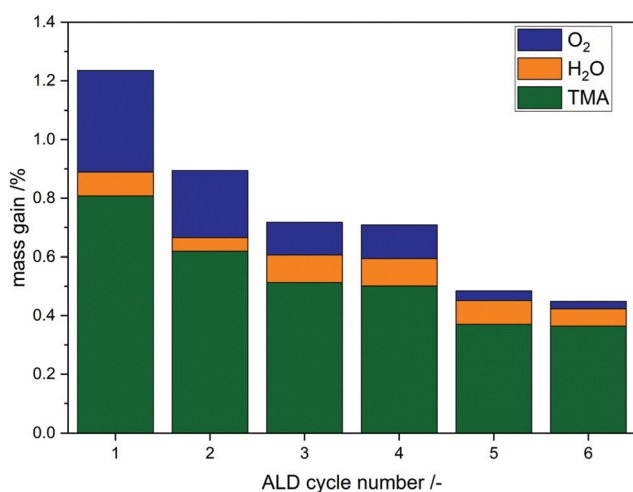
theoretical coverage of one monolayer,[16] which explains the loss of mass uptake due to oxygen. With XRF the mass uptake of Al was determined in the first cycle to be 0.65 wt% resulting in 37.5 Al nm^{-2} assuming Frank–van-der-Merwe growth. Correlating the surface density of aluminum to the surface hydroxyl groups (1.4 OH nm^{-2}) results in a ratio of Al/OH = 26.8. Therefore, ALD on divanadium pentoxide does not exclusively proceed over surface hydroxyl groups, but an additional mechanism must be present. Comparing the Al coverage to available surface vanadium atoms leads to the ratio Al/V = 3.8, meaning a theoretical deposition above one monolayer. Despite the high Al/V ratio, STEM-EDX shows homogeneously distributed Al after 1 cycle and 6 cycles (ESI,† Fig. S7 and S8). In addition, XRD does not detect any crystallites, which would lead to the assumption of island growth (ESI,† Fig. S9). This has to be carefully interpreted, as deposition above one monolayer within one cycle is not typical for ALD, but rather for uncontrolled chemical vapor deposition. Self-limitation is achieved in each half cycle as the mass does not change over time despite the presence of precursor.
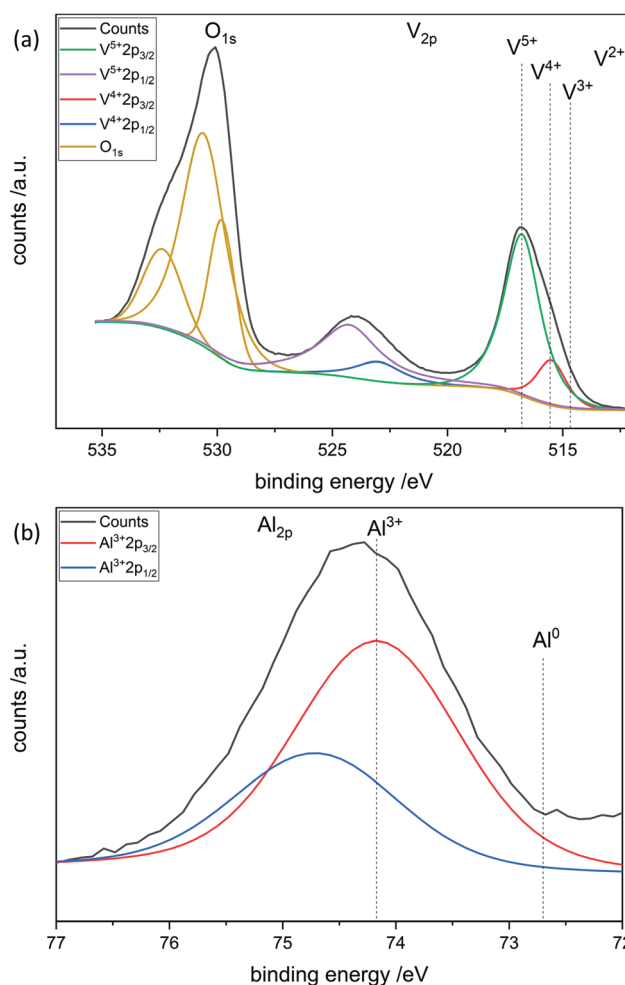

Fig. 8   XPS of AlO_x/V_2O_5 after the first half cycle of AlO_x-ALD. (a) O_{1s}, V_{2p} and (b) Al_{2p} spectra.

Fig. 7   Mass uptake distribution of each step during the first 6 cycles for the reaction sequence $TMA-H_2O-O_2(450 \ °C)$.

18004 | *Phys. Chem. Chem. Phys.*, 2020, **22**, 17999–18006

This journal is © the Owner Societies 2020

Table 3 XPS summary of AlO_x ALD on V_2O_5 during each synthesis step in the first cycle and the determined ratio R

	R
V_2O_5 fresh	0.16
V_2O_5 calcined (450 °C)	0.11
AlO_x/V_2O_5 1 half cycle	0.40
AlO_x/V_2O_5 1 cycle (150 °C)	0.17
AlO_x/V_2O_5 1 cycle (450 °C)	0.20

Here, the limiting factor most likely is not the initial amount of reactive surface sites but rather the diffusion of bulk oxygen to the surface. The literature shows that after surface vanadyl groups are consumed they can be regenerated to a certain degree by bulk vanadyl groups due to oxygen diffusion.[42] This fact might explain the high Al loading, as reactive oxygen species are provided during the reaction not only from the surface but also from the bulk, still leading to self-limitation at one point. As in the phosphorus system, the color changes from orange to green in the first half cycle and back to orange at 450 °C in oxygen which indicates redox chemistry (ESI,† Fig. S10). In addition, a high mass uptake during the oxygen cycle results due to the filling of defect sites in the vanadia structure.

XPS was performed at each step during the synthesis in the first complete cycle (Fig. 8). It can be seen that adding TMA leads to the reduction of divanadium pentoxide as indicated by the ratio R (Table 3). Dosing water barely changes the oxidation states of the vanadium species. However, heating in oxygen to 450 °C leads to complete oxidation of the vanadium oxide. Aluminum always remains in its maximum oxidation state Al^{3+}. This leads to the conclusion that the carbons of the ligand are oxidized while the vanadium is reduced from V^{5+} to V^{4+}. Mass spectrometry reveals that TMA reacts with vanadium oxide to form methane most likely over the surface hydroxyl groups. In addition, electron transfer from the methyl group to vanadium occurs, as ethane is evolving, in which the carbon in $Al–CH_3$ transitions from C^{4-} to C^{3-} in ethane (ESI,† Fig. S11).
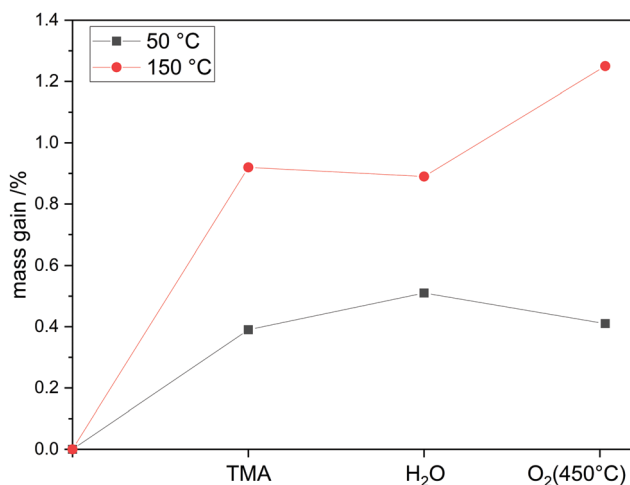
This is in contrast to the phosphorus system in which the central atom is oxidized whereas in the aluminum system the ligands are oxidized. The mass uptake during the thermal treatment at 450 °C is therefore an indicator of redox chemistry on divanadium pentoxide, as the mass change is the sum of oxygen incorporation into vanadium oxide (mass uptake) and the loss of ligands due to combustion (mass loss). If there is a mass uptake in this step, redox chemistry occurs. Performing the aluminum oxide ALD at lower temperatures, such as 50 °C, thermal treatment at 450 °C in oxygen does not result in mass uptake, indicating that redox chemistry can be suppressed by lowering the temperature (Fig. 9). In addition, the reaction time until saturation decreased by 80% from 21.3 h g^{-1} to 4.2 h g^{-1}.

Conclusions

We successfully developed an ALD process to deposit phosphorus oxide on divanadium pentoxide by investigating the reaction mechanism with combined *in situ* analytics. XRF showed P loadings exceeding the surface hydroxyl group density, leading to the conclusion of additional reactive surface sites being present. During the deposition process redox reaction takes place, in which the P^{3+} precursor oxidized to P^{5+} and V^{5+} is reduced to V^{4+} as revealed by XPS. High temperatures of 450 °C in the oxygen cycle are needed to obtain linear growth per cycle because remaining ligands need to be combusted and reduced vanadium atoms need to be reoxidized. STEM-EDX mappings show homogeneously distributed phosphorus on the surface and XRD could not detect additional phases.

Further investigations were made by depositing TMA/H_2O on divanadium pentoxide by the literature known process. Again, XPS confirms the presence of redox chemistry for alumina ALD at 150 °C. This reaction can be controlled by lowering the deposition temperature to 50 °C. Performing ALD on an oxidation catalyst is clearly different from ALD on inert supports. Unusual growth behaviour occurred during both processes and they were successfully controlled by adjusting the deposition parameters accordingly. The knowledge about possible reaction mechanisms and how to control them allows the development of further ALD processes on additional bulk catalysts in future.

Conflicts of interest

There are no conflicts to declare.

Acknowledgements

Fig. 9 ALD of AlO_x on V_2O_5 at 50 °C and 150 °C with the reaction sequence $TMA–H_2O–O_2$(450 °C).

This journal is © the Owner Societies 2020

Phys. Chem. Chem. Phys., 2020, **22**, 17999–18006 | **18005**

Notes and references

1 T. Dobbelaere, F. Mattelaer, P. M. Vereecken and C. Detavernier, *J. Vac. Sci. Technol., A*, 2017, **35**, 041513.

2 X. Meng, X. Q. Yang and X. Sun, *Adv. Mater.*, 2012, **24**, 3589–3615.

3 Y. Zhao, K. Zheng and X. Sun, *Joule*, 2018, **2**, 2583–2604.

4 J. Lu, J. W. Elam and P. C. Stair, *Surf. Sci. Rep.*, 2016, **71**, 410–472.

5 R. L. Puurunen, *J. Appl. Phys.*, 2005, **97**, 121301.

6 W. J. Lee, S. Bera, H. C. Shin, W. P. Hong, S. J. Oh, Z. Wan and S. H. Kwon, *Adv. Mater. Interfaces*, 2019, **6**, 1–9.

7 V. R. Anderson, N. Leick, J. W. Clancey, K. E. Hurst, K. M. Jones, A. C. Dillon and S. M. George, *J. Phys. Chem. C*, 2014, **118**, 8960–8970.

8 A. J. M. Mackus, M. J. Weber, N. F. W. Thissen, D. Garcia-Alonso, R. H. J. Vervuurt, S. Assali, A. A. Bol, M. A. Verheijen and W. M. M. Kessels, *Nanotechnology*, 2015, **27**, 34001.

9 H. Feng, J. W. Elam, J. A. Libera, M. J. Pellin and P. C. Stair, *J. Catal.*, 2010, **269**, 421–431.

10 N. Yan, L. Qin, J. Li, F. Zhao and H. Feng, *Appl. Surf. Sci.*, 2018, **451**, 155–161.

11 S. Haschke, D. Pankin, Y. Petrov, S. Bochmann, A. Manshina and J. Bachmann, *ChemSusChem*, 2017, **10**, 3644–3651.

12 N. Cheng, M. N. Banis, J. Liu, A. Riese, X. Li, R. Li, S. Ye, S. Knights and X. Sun, *Adv. Mater.*, 2015, **27**, 277–281.

13 W. Yang, Z. Lu, B. Vogler, T. Wu and Y. Lei, *ACS Appl. Mater. Interfaces*, 2018, **10**, 43323–43326.

14 E. Langereis, S. B. S. Heil, H. C. M. Knoops, W. Keuning, M. C. M. van de Sanden and W. M. M. Kessels, *J. Phys. D: Appl. Phys.*, 2009, **42**, 073001.

15 K. Knapas and M. Ritala, *Crit. Rev. Solid State Mater. Sci.*, 2013, **38**, 167–202.

16 V. E. Strempel, R. Naumann D'Alnoncourt, M. Driess and F. Rosowski, *Rev. Sci. Instrum.*, 2017, **88**, 074102.

17 J. H. Lee, A. Mirzaei, J. H. Kim, J. Y. Kim, A. F. Nasriddinov, M. N. Rumyantseva, H. W. Kim and S. S. Kim, *Sens. Actuators, B*, 2020, **310**, 127870.

18 V. E. Strempel, D. Löffler, J. Kröhnert, K. Skorupska, B. Johnson, R. N. D'Alnoncourt, M. Driess and F. Rosowski, *J. Vac. Sci. Technol., A*, 2016, **34**, 01A135.

19 S. C. Riha, B. M. Klahr, E. C. Tyo, S. Seifert, S. Vajda, M. J. Pellin, T. W. Hamann and A. B. F. Martinson, *ACS Nano*, 2013, **7**, 2396–2405.

20 H. Yan, H. Cheng, H. Yi, Y. Lin, T. Yao, C. Wang, J. Li, S. Wei, J. Lu, H. Yan, H. Cheng, H. Yi, Y. Lin, T. Yao, C. Wang, J. Li and S. Wei, *J. Am. Chem. Soc.*, 2015, 1–6.

21 B. J. Oneill, D. H. K. Jackson, J. Lee, C. Canlas, P. C. Stair, C. L. Marshall, J. W. Elam, T. F. Kuech, J. A. Dumesic and G. W. Huber, *ACS Catal.*, 2015, **5**, 1804–1825.

22 J. W. Elam, A. V. Zinovev, M. J. Pellin, D. J. Comstock and M. C. Hersam, *ECS Trans.*, 2007, **3**, 271–278.

23 J. Hämäläinen, M. Ritala and M. Leskelä, *Chem. Mater.*, 2014, **26**, 786–801.

24 D. Valdesueiro, M. K. Prabhu, C. Guerra-Nunez, C. S. S. Sandeep, S. Kinge, L. D. A. Siebbeles, L. C. P. M. De Smet, G. M. H. Meesters, M. T. Kreutzer, A. J. Houtepen and J. R. V. Ommen, *J. Phys. Chem. C*, 2016, **120**, 4266–4275.

25 W. Setthapun, W. D. Williams, S. M. Kim, H. Feng, J. W. Elam, F. A. Rabuffetti, K. R. Poeppelmeier, P. C. Stair, E. A. Stach, F. H. Ribeiro, J. T. Miller and C. L. Marshall, *J. Phys. Chem. C*, 2010, **114**, 9758–9771.

26 T. D. Gould, A. M. Lubers, A. R. Corpuz, A. W. Weimer, J. L. Falconer and J. W. Medlin, *ACS Catal.*, 2015, **5**, 1344–1352.

27 P. Schindler, M. Logar, J. Provine and F. B. Prinz, *Langmuir*, 2015, **31**, 5057–5062.

28 U. Cvelbar, M. Mozetič and A. Ricard, *IEEE Trans. Plasma Sci.*, 2005, **33**, 834–837.

29 V. E. Strempel, K. Knemeyer, R. N. D'Alnoncourt, M. Driess and F. Rosowski, *Nanomaterials*, 2018, **8**, 365.

30 J. Lu, B. Fu, M. C. Kung, G. Xiao, J. W. Elam, H. H. Kung and P. C. Stair, *Science*, 2012, **335**, 1205–1209.

31 F. C. Frank and J. H. Van Der Merwe, *Proc. R. Soc. London, Ser. A*, 1949, **198**, 216–225.

32 J. Haber, M. Witko and R. Tokarz, *Appl. Catal., A*, 1997, **157**, 3–22.

33 R. Wojcieszak, M. J. Genet, P. Eloy, P. Ruiz and E. M. Gaigneaux, *J. Phys. Chem. C*, 2010, **114**, 16677–16684.

34 R. L. Puurunen, W. Vandervorst, W. F. A. Besling, O. Richard, H. Bender, T. Conard, C. Zhao, A. Delabie, M. Caymax, S. De Gendt, M. Heyns, M. M. Viitanen, M. De Ridder, H. H. Brongersma, Y. Tamminga, T. Dao, T. De Win, M. Verheijen, M. Kaiser and M. Tuominen, *J. Appl. Phys.*, 2004, **96**, 4878–4889.

35 J. W. Elam, C. E. Nelson, R. K. Grubbs and S. M. George, *Thin Solid Films*, 2001, **386**, 41–52.

36 R. L. Puurunen and W. Vandervorst, *J. Appl. Phys.*, 2004, **96**, 7686–7695.

37 O. Nilsen, C. E. Mohn, A. Kjekshus and H. Fjellvåg, *J. Appl. Phys.*, 2007, **102**, 024906.

38 J. W. Elam, A. V. V. Zinovev, M. J. Pellin, D. J. Comstock and M. C. Hersam, *ECS Trans.*, 2019, **3**, 271–278.

39 M. T. Sananes, A. Tuel and J. C. Volta, *J. Catal.*, 1994, **145**, 251–255.

40 K. Hermann, M. Witko, R. Druzinic and R. Tokarz, *Appl. Phys. A: Mater. Sci. Process.*, 2001, **72**, 429–442.

41 R. T. J. Haber and M. Witko, *Appl. Catal., A*, 1997, **157**, 3–22.

42 A. Miyamoto, Y. Yamazaki, M. Inomata and Y. Murakami, *J. Phys. Chem.*, 1981, **85**, 2366–2372.